Article

Clay Mineral Suites in Submarine Mud Volcanoes in the Kumano Forearc Basin, Nankai Trough: Constraints on the Origin of Mud Volcano Sediments

Akira Ijiri [1,2,*], Koichi Iijima [2], Urumu Tsunogai [3] , Juichiro Ashi [4] and Fumio Inagaki [1,2,5]

[1]   Kochi Institute for Core Sample Research, Japan Agency for Marine-Earth Science and
      Technology (JAMSTEC), Nankoku, Kochi 783-8502, Japan; inagaki@jamstec.go.jp
[2]   Research and Development Center for Submarine Resources, JAMSTEC, Yokosuka,
      Kanagawa 237-0061, Japan; kiijima@jamstec.go.jp
[3]   Graduate School of Environmental Studies, Nagoya University, Nagoya 464-8601, Japan;
      urumu@nagoya-u.jp
[4]   Atmosphere and Ocean Research Institute, The University of Tokyo, Kashiwa, Chiba 277-0885, Japan;
      ashi@aori.u-tokyo.ac.jp
[5]   Research and Development Center for Ocean Drilling Science, JAMSTEC, Yokohama,
      Kanagawa 236-0001, Japan
*   Correspondence: ijiri@jamstec.go.jp; Tel.: +81-88-783-8199

check for updates

Abstract: Clay mineralogy is an important characteristic of mud volcano sediments. This study determined the clay mineral compositions of sediment from two submarine mud volcanoes in the Kumano forearc basin, Nankai Trough, by X-ray diffraction analysis. Similar compositions dominated by smectite in the two mud volcanoes indicate that the mud volcanoes in the basin are rooted in the same source sequence. These clay mineral compositions differed from those in Pleistocene basin sediment, suggesting that the mud volcano sediment originated beneath the Pleistocene sediment. The illite content in the illite–smectite mixed layer averaged 32% in the mud volcano sediment, which implies that the sediment experienced temperatures above 60 °C that promoted the smectite-to-illite transformation. However, porewater extracted from the mud volcano sediment had Cl⁻ concentrations roughly half that of seawater and proportional enrichment in ^{18}O and depletion in D, indicating that dehydration reactions of clay minerals had previously occurred in a deeply buried sedimentary layer. The smectite and illite contents (<60%) in the clay-size fraction rule out in situ smectite dewatering as the cause of the dilution of Cl⁻ in porewater. Thus, fluids derived from clay dewatering must have originated from deeper than the source of the mud volcano sediment.

Keywords: mud volcano; clay mineral; porewater

1. Introduction

Submarine mud volcanoes are remarkable seafloor features that consist of mud breccia derived from sediment layers beneath the seafloor [1]. They form by expulsions of mud and associated deep-sourced fluids, predominantly methane gas [2,3]. The origin and composition of these fluids have been the subjects of many studies (e.g., [4–7]). These studies have shown that the fluids commonly originate from dehydration reactions of clay minerals. The fluids also contain hydrocarbon gases derived from the thermocatalytic decomposition of organic matter (e.g., [6–8]). These characteristics suggest that the fluids originate at depths where temperatures are high enough to promote these reactions. However, there are fewer lithological studies that include chemical and mineralogical analyses of mud volcano sediments than there are studies of mud volcano fluids (e.g., [9–11]), although

the lithology of erupted sediment is strongly related to the formation of mud volcanoes and the source of their sediments. Given the large proportion of clay in submarine mud volcanoes, clay mineralogy is an important characteristic of mud volcano sediments, particularly signs of clay mineral dehydration that is an important proxy for the thermal history of sediments [9]. This paper reports the clay mineralogy and porewater chemistry of sediment from mud volcanoes in the northern part of the Kumano forearc basin, in the Nankai Trough, and compares these results to previously reported data from sediment sampled during scientific drilling in the Nankai Trough. Although the fluid and gas chemistry at these mud volcanoes has been studied [8,12–14], the clay mineralogy of the mud volcano sediments has not been investigated.

2. Geologic Setting and Previous Studies

The Kumano Basin, located southeast of the Kii Peninsula, is a forearc basin in the Nankai Trough, where the Philippine Sea plate is subducting beneath the Eurasia plate (Figure 1). The basin floor, at a water depth of approximately 2100 m, overlies a thick sequence (up to 2000 m) of terrigenous and hemipelagic sediment [12]. Thirteen mud volcanoes have been mapped on anticlines above landward-dipping megasplay faults related to the subduction zone and have been assigned "Kumano mud volcano numbers" (KMV#) from 1 to 13 [8,12–14] (Figure 1). At KMV#2, KMV#4, KMV#5, and KMV#10, the carbon isotopic compositions of methane and the methane to (ethane + propane) concentration ratios in the hydrate-bound hydrocarbons have been analyzed [8]. These data suggest that the hydrocarbon gases are derived from thermal cracking of organic matter in the old accretionary prism underlying the Kumano forearc basin sediment. The oxygen and hydrogen isotopic compositions of porewater retrieved from 10 of these mud volcanoes (KMV#2–11) have suggested that the fluid in the mud volcanoes was derived from dehydration of clay minerals in the old accretionary prism [13]. KMV#5 is the most intensively surveyed mud volcano in the Kumano basin. Core drilling in 2009 and 2012 by deep-sea drilling vessel *Chikyu* reached 200 m below the summit of KMV#5 and revealed the existence of methane hydrate in the erupted sediments [15]. Although the oxygen and hydrogen isotopic compositions of porewater were affected by dissociation of methane hydrate, the inferred original isotopic composition was consistent with fluid derived from clay mineral dehydration in the old accretionary prism [13]. In addition, the lithium isotopic composition of porewater extracted from the drilled sediment showed that a portion of the fluid originated in the corner of the serpentinized forearc mantle wedge [16]. In contrast, nannofossils in the shallow sediment at KMV#5 retrieved by piston coring during 2001–2002 are of younger origin, dating from the late early to early middle Miocene (13.6–18.2 Ma), which implies that the mud is from the bottom of the forearc basin, not from the older underlying accretionary prism [12].

3. Materials and Methods

3.1. Sediment Cores

During cruise KH-06-03 of R/V *Hakuho Maru* in 2006, piston cores were retrieved from two mud volcanoes in the Kumano basin: core PC13 from KMV#5 (33°40.618′ N, 136°34.007′ E; water depth 1899 m; total core length 176.2 cm), and core PC14 from KMV#10 (33°32.813′ N, 136°17.030′ E; water depth 1849 m; total core length 238 cm). A reference core (PC12) was retrieved during this cruise at the boundary between the northern part of the Kumano Basin and the foot of the continental slope (33°51.30′ N, 136°19.99′ E; water depth 1891 m; total core length 256.6 cm) (Figure 1).
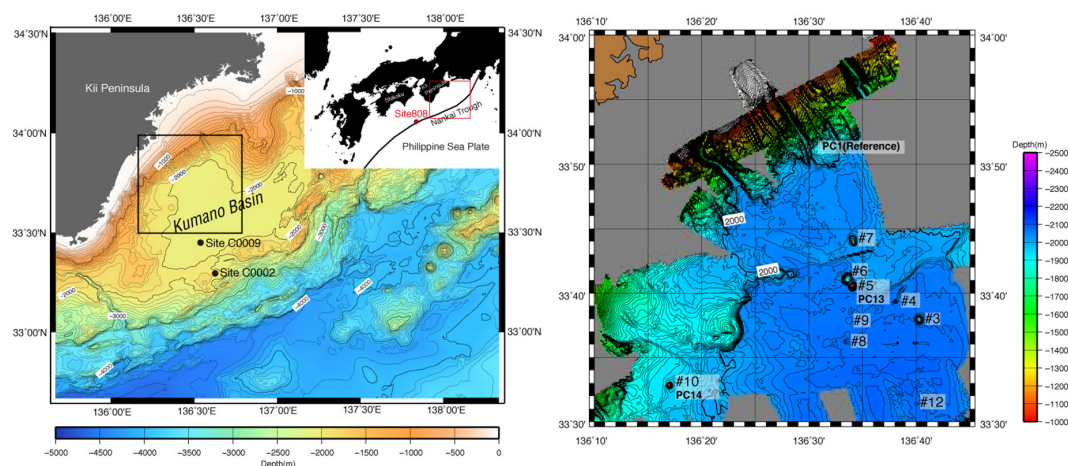
Figure 1. Location map of the Kumano basin showing core sites PC12 (reference site), PC13 (KMV#5), and PC14 (KMV#10), and IODP and ODP Sites. Numbers with # indicate the locations of KMV#3–10 and KMV#12.

3.2. Porewater Samples

Sediment samples of about 500 cm^3 (10 cm length of whole round core samples) were collected from the cores at 50-cm intervals, and porewater was extracted from them on board using a stainless steel squeezer [17].

The Cl$^-$ concentration in the porewater samples was analyzed by using an ion chromatograph (Dionex DX-500) with an isocratic carbonate/bicarbonate eluent coupled with suppressed conductivity detection and an IonPac AS12A carbonate eluent anion-exchange column (200 mm long, 4 mm i.d.; Dionex, Sunnyvale, CA, USA) equipped with a guard column (IonPac AG12A, 50 mm long, 4 mm i.d.; Dionex). Analytical precision was estimated to be within 0.3% from repeated measurements of the same samples.

For δ^{18}O measurements, porewater samples were analyzed by using a stable isotope ratio mass spectrometer (GV IsoPrime, GV Instruments Ltd., Wythenshawe, UK) with an automated CO_2-H_2O equilibration system (GV MultiPrep). The external precision (1σ) was ± 0.05‰.

For δD measurements, porewater samples were injected into an online chromium reduction analytical system attached to an isotope ratio mass spectrometer (VG SIRA10, VG Isogas Ltd., Middlewich, UK) [18]. For each analysis, a 2-μL water sample was injected into a quartz furnace containing chromium metal powder at 800 °C. The external precision (1σ) was ± 0.4‰.

3.3. Clay Mineral Assemblage

For X-ray diffraction (XRD) analysis, sediment samples of about 5 cm^3 were collected by a tip cut disposable syringe from the top of the same whole round core samples used for porewater extraction. The clay-size fraction (<2 μm) was separated from the sediment samples by centrifugation [19] at 1500 rpm for 1 min. The size of the clay-size fraction was determined by weighing the dried bulk sediment sample and the separated clay-size fraction; note that this is a minimum value, because the recovery rate of the clay-size fraction by centrifugation is not 100%.

The mineralogy of the clay-size fractions was determined by X-ray diffraction (XRD) analysis. Suspensions of clay were dropped onto glass slides and dried in an oven at 50 °C to prepare oriented samples. XRD patterns of these samples were obtained using an X-ray diffractometer (MacScience, MXP3HF) with CuKα radiation at 40 kV and 20 mA, with 1° divergence and antiscattering slits and a 0.15 mm receiving slit. The diffracted X-rays were counted for 2 s at steps of 0.02° in 2θ. The samples were then saturated with ethylene glycol vapor at 50 °C for 5 h and the XRD scanning was repeated. For each sample, ethylene glycol vapor saturation and XRD scanning were performed twice.

The proportions of major minerals in the clay-size fraction were semiquantitatively estimated from the XRD data by measurement of peak areas and application of the calibrated weighting factors reported by Underwood et al. [20] (Supplementary Table S1). A matrix of weighting factors was applied to the integrated areas of a smectite(001) peak at $2\theta \approx 5.5°$, the illite(001) peak at $2\theta \approx 9°$, the chlorite(002) + kaolinite(001) peak at $2\theta \approx 12.5°$, and the quartz(100) peak at $2\theta \approx 20.9°$. The proportions of major clay minerals in the clay-size fraction were also semiquantitatively estimated by the methods of Biscaye [21], the most commonly used approach to calculate the relative proportions of smectite, illite, and chlorite in marine geology. However, errors in such data can be substantial, and accuracy changes significantly in response to the abundance by weight of each mineral [19,20]. To avoid these errors, Underwood et al. [20] introduced a normalization factor in which the weighting factors are calculated independently for each mineral (Supplementary Table S1). However, the estimates made by the Underwood method are also semiquantitative in light of limitations imposed by differences in indigenous mineral mixtures, X-ray diffractometers (e.g., scanning mode and slits), and the individual instrument performance [20].

The proportions of illite and smectite crystallites in the illite/smectite (I/S)-mixed-layer layers were calculated using the angular separation ($\Delta°2\theta$) between the composite illite(001)/smectite(002) reflection at $2\theta \approx 10.5°$ and the composite illite(002)/smectite(003) reflection at $2\theta \approx 16°$ [22]. The saddle/peak method [23], based on the intensity ratio of illite(001)–smectite(001) peak at $2\theta \approx 5.5°$ to the background intensity at smaller angles ("saddle"), was used to calculate the percent expandability of smectite and the I/S mixed layer on the basis of a curve established for 1:1 mixtures of illite and I/S. The Sharpness Ratio, an indicator of illite crystallinity defined as the intensity ratio of illite(001) at 10.0 Å ($2\theta \approx 9°$) to the intensity at 10.5 Å ($2\theta \approx 8.4°$), was also determined [24].

4. Results

4.1. Porewater Chemistry

At the reference site (PC12), the Cl$^-$ concentration in porewater at all depths was essentially constant at 543–558 mM (Figure 2a). Porewater Cl$^-$ concentrations at KMV#5 and KMV#10 (PC13 and PC14, respectively) were much lower than that of seawater (ca. 550 mM), decreasing with depth in the cores to minimums of 280 mM at KMV#5 and 471 mM at KMV#10 at the bottom of the cores.

Oxygen isotopic compositions (δ^{18}O) of porewater increased with increasing depth at both KMV#5 and KMV#10 (Figure 2b), and hydrogen isotopic ratios (δD) decreased with increasing depth (Figure 2c). The plot of δ^{18}O against Cl$^-$ concentration shows ^{18}O enrichment proportional to Cl$^-$ depletion. The plot of δD against Cl$^-$ concentration shows D depletion proportional to Cl$^-$ depletion (Figure 3).
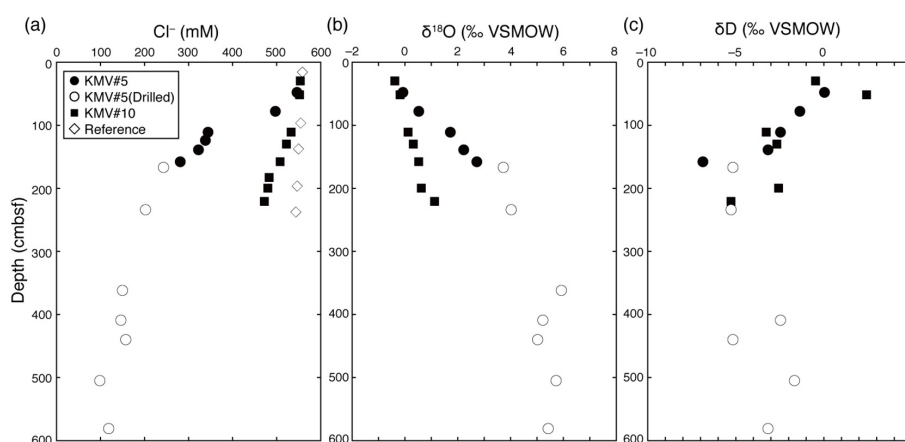

Figure 2. Vertical profiles of (**a**) Cl$^-$ concentrations, (**b**) δ^{18}O and (**c**) δD in porewater samples from this study and the drilled core from KMV#5 [15]. VSMOW, Vienna Standard Mean Ocean Water.
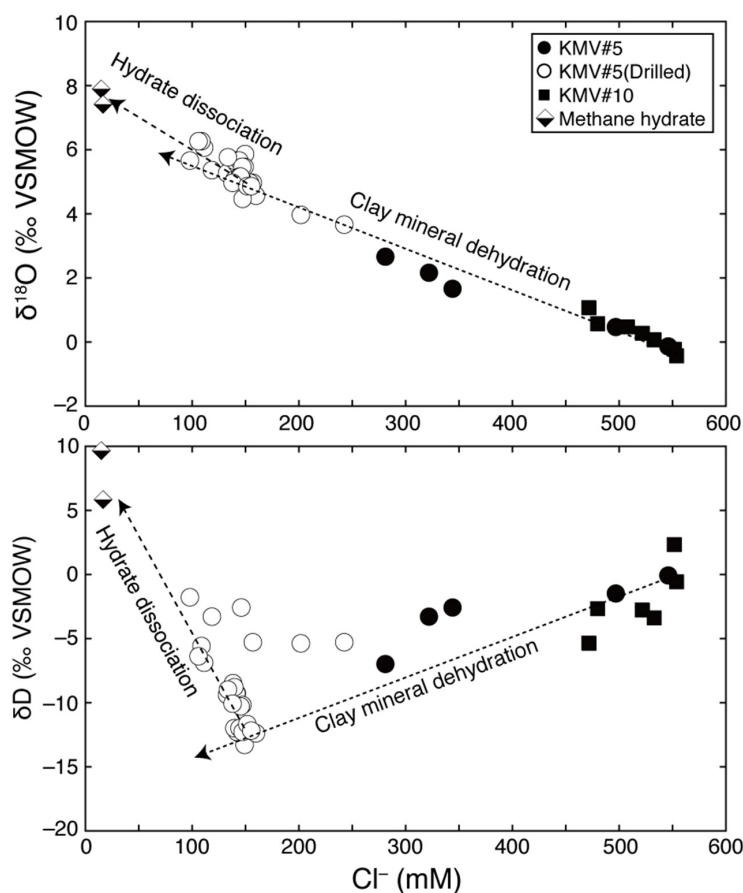
Figure 3. Relationships of $\delta^{18}O$ vs. Cl⁻ (**top**) and δD vs. Cl⁻ (**bottom**) in the samples from this study and in the drilled core from KMV#5 [15]. Also shown are isotopic data from water obtained from methane hydrate dissociation.

4.2. Clay Mineral Assemblage

A total of 23 samples were analyzed by XRD. Figure 4 shows representative examples of X-ray diffractograms for the samples in the ethylene-glycolated state from KMV#5, KMV#10, and the reference site.

The X-ray diffractograms of the samples from KMV#5 and KMV#10 showed similar patterns. These displayed strong intensity peaks at $2\theta \approx 5.5°$, representing a mixture of discrete smectite and I/S mixed-layer. The composite reflection of illite(002)/smectite(003) at $2\theta \approx 16°$ was detected. The peak intensities of the peaks at $2\theta \approx 9°$ representing illite(001), and the overlapped peak of chlorite(002) and kaolinite(001) at $2\theta \approx 12.5°$ were low. We could not identify the kaolinite(002) peak at 24–26° in the samples from KMV#5 and the reference site (Figure 5). In the samples from KMV#10, we identified a small contribution of kaolinite(002) in the peak at 24–26° and decomposed this peak into elementary peaks of kaolinite(002) and chlorite(004) using Profile Fit Software (Philips PROFIT v.1.0). The intensity ratios of kaolinite(002)/chlorite(004) were less than 0.07 (Table 1). These observations indicate small contents of kaolinite in the studied samples.

The peak intensities in the X-ray diffractogram of the reference-site sample were much lower than those of the mud volcano sediments (Figure 4). The smectite peak at $2\theta \approx 5.5°$ was subtle.

The clay-size fraction (<2 μm) made up 1.8–12.2 wt % of the sediment at KMV#5 and KMV#10 and 1.6–3.5 wt % of the reference sediment (Figure 6; Table 1). In the mud volcano sediments, the clay-size fraction increased from 2% to 7% near the surface to 12% at the bottom of the cores.

The relative percentages of dominant clay minerals and quartz in the clay-size fraction, estimated following Underwood et al. [20], are shown in Figure 6 and listed in Table 1. Chlorite concentrations were estimated from the integrated peak area of the isolated chlorite(001) peak at $2\theta \approx 13.5°$. At KMV#5 and KMV#10, the clay-size fraction consisted of 41–59% smectite (average 49%), 23–29% illite (average 25%), 7–15% chlorite (average 11%), and 8–24% quartz (average 15%). Sediment at the reference site consisted of 21–24% smectite (average 23%), 28–35% illite (average 30%), 17–18% chlorite (average 18%), and 26–32% quartz (average 29%). The method of Biscaye [21] yielded higher illite concentrations than the method of Underwood et al. [20] (Table 1), a result consistent with previous reports [20].

The illite content in the I/S mixed layer was estimated only for the mud volcano sediments, because the composite reflections of illite(001)/smectite(002) and illite(002)/smectite(003) were absent in the X-ray diffractograms for the samples from the reference site. At KMV#5 and KMV#10, the inferred illite contents in the I/S mixed layer ranged from 19% to 38% (average 32%) (Figure 7a).

Expandability was estimated only for the mud volcano sediments because the saddle/peak ratio could not be determined in the reference sediment. The expandability values increased from 61% to 70%, with increasing depth in the cores, and averaged 67% in the mud volcano sediments (Figure 7b).

The Weaver's Sharpness Ratio ranged from 3.3 to 5.5 for the mud volcano sediments and from 2.8 to 3.8 for the reference-site sample (Figure 7c).
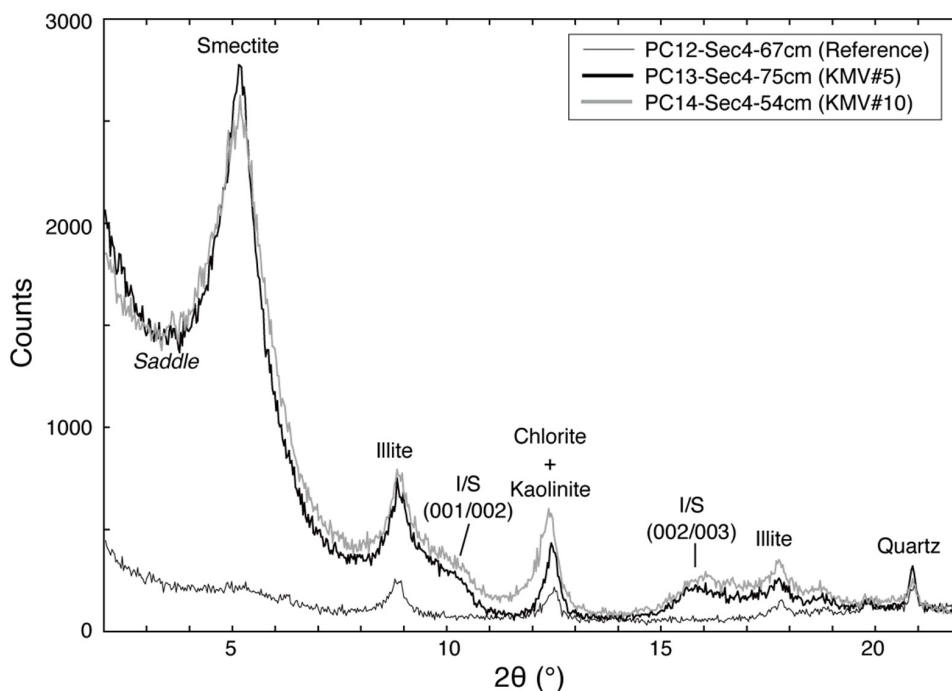

Figure 4. Representative X-ray diffractograms of clay size fractions in the ethylene-glycolated state from KMV#5 (PC13-Sec4-75 cm, 157 cmbsf), KMV#10 (PC14-Sec4-54 cm, 182 cmbsf) and reference site (PC12-Sec4-67 cm, 237 cmbsf).
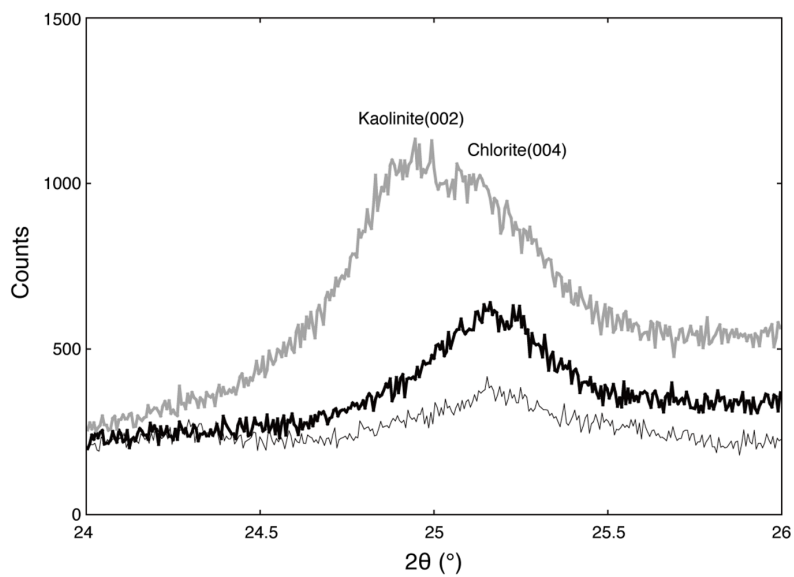
Figure 5. Representative kaolinite(002) and chlorite(004) peaks in the X-ray diffractograms ($2\theta = 24$–$26°$) of clay size in the ethylene-glycolated state from this study.

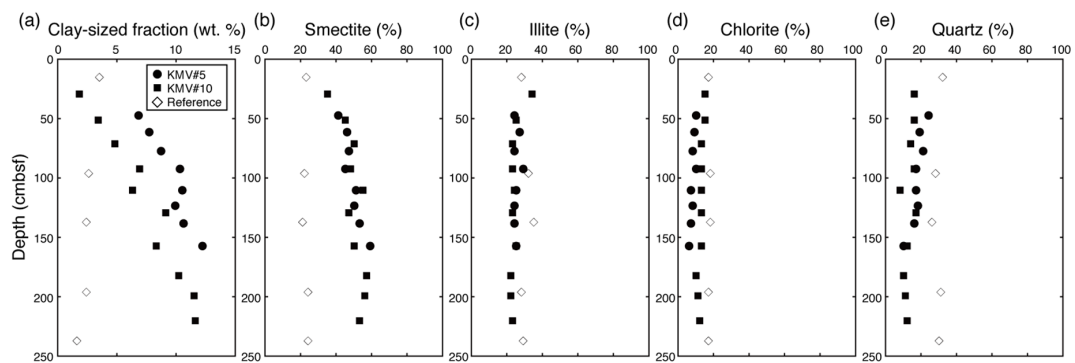**Figure 6.** Vertical profiles of (**a**) clay-size fractions and percentages of (**b**) smectite, (**c**) illite, (**d**) chlorite and (**e**) quartz from this study.
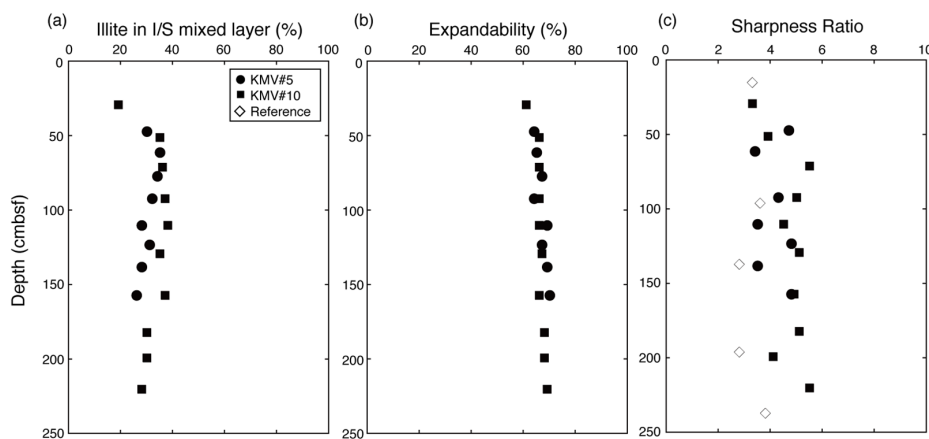

Figure 7. Vertical profiles of (**a**) illite in the I/S mixed layer; (**b**) expandability in clay-size fractions from KMV#5 and KMV#10 and (**c**) Weaver's Sharpness Ratio for the mud-volcano sediments and the reference-site sample.

Table 1. Clay mineralogy of samples from the reference site, KMV#5, and KMV#10 (I, illite; S, smectite; C, chlorite; K, kaolinite; Q, quartz).

		Integrated Peak Area (Counts)								Estimated Mineral Abundance in Clay-Size Fraction						
										Biscaye [21] Factors			Guo and Underwood [19] Factors			
Site	Sample Name	Depth	S	I	C(002)	Q	K	C	K(004)/C(002)	S	I	C + K	S	I	C	Q
		(cmbsf)	(001)	(001)	+K(001)	(001)	(002)	(004)		(%)	(%)	(%)	(%)	(%)	(%)	(%)
Reference site	PC12-Sec2-76 cm	15	1146	2334	2098	1206	-	-	-	8	64	29	23	28	17	32
	PC12-Sec3-26 cm	96	1749	2794	2314	1029	-	-	-	10	64	26	22	32	18	28
	PC12-Sec4-26 cm	196	1606	2269	1994	1100	-	-	-	11	62	27	24	28	17	31
	PC12-Sec4-67 cm	137	1759	3093	2375	919	-	-	-	9	66	25	21	35	18	26
	PC12-Sec4-67B cm	237	1827	2645	2237	1173	-	-	-	11	63	27	24	29	17	30
KMV#5	PC13-Sec3-43 cm	47	26,884	6693	3869	3346	-	-	-	44	44	13	41	24	10	24
	PC13-Sec3-57 cm	61	48,162	11,047	5524	3822	-	-	-	47	43	11	46	27	9	19
	PC13-Sec3-71 cm	77	45,563	8978	4254	4080	-	-	-	51	40	9	47	24	8	21
	PC13-Sec4-10 cm	92	30,761	7863	4031	2231	-	-	-	44	45	11	45	29	10	17
	PC13-Sec4-28 cm	110	63,384	11,482	5167	3946	-	-	-	53	38	9	51	25	7	17
	PC13-Sec4-41 cm	123	53,183	9737	4570	3785	-	-	-	52	39	9	50	24	8	18
	PC13-Sec4-56 cm	138	49,218	8262	3856	2928	-	-	-	55	37	9	53	24	7	16
	PC13-Sec4-75 cm	157	68,306	10,639	5223	2633	-	-	-	56	35	9	59	25	6	10
KMV#10	PC14-Sec2-25 cm	29	12,365	5105	3524	1070	-	-	-	31	51	18	35	34	15	16
	PC14-Sec3-6 cm	51	36,796	7726	7674	2415	-	-	-	44	37	18	45	25	15	16
	PC14-Sec3-26 cm	71	49,275	8001	7989	2626	2824	47,814	0.059	51	33	16	50	23	13	14
	PC14-Sec3-47 cm	92	49,574	8841	8680	3088	3419	51,595	0.066	48	35	17	48	23	13	16
	PC14-Sec3-65 cm	110	57,633	9162	8816	2025	2417	50,794	0.048	51	33	16	55	24	13	8
	PC14-Sec4-12 cm	129	46,329	8454	8200	3199	2840	57,185	0.050	48	35	17	47	23	13	17
	PC14-Sec4-37 cm	157	56,447	10,272	9386	2677	3284	56,266	0.058	48	35	16	50	25	13	12
	PC14-Sec4-54 cm	182	70,632	9904	8040	2859	2830	46,804	0.060	56	31	13	57	22	10	10
	PC14-Sec4-75 cm	199	72,661	10,264	8789	3156	3265	51,381	0.064	55	31	13	56	22	11	11
	PC14-Sec4-84 cm	220	61,886	9713	8504	2873	2346	55,604	0.042	53	33	14	53	23	12	12

5. Discussion

The porewater samples from the Kumano mud volcanoes can be characterized by depletion of Cl⁻ relative to the reference sediment of the Kumano basin, indicating the mixing of a freshwater component. At KMV#5, the Cl⁻ concentration in porewater extracted from the drilled core was constant at ca. 130–150 mM from 4 m depth in the core to the core bottom (120 m) [15]. In the drilled core, $\delta^{18}O$ and δD values generally shifted with depth toward high and low values relative to seawater, respectively (Figure 3). Conversely, $\delta^{18}O$ and δD values of water obtained from methane hydrate were higher than those of porewater. Ijiri et al. [15] estimated that the original $\delta^{18}O$ and δD values of porewater before methane hydrate formation were +4.3‰–+5.3‰ and −9.2‰−−16.2‰, respectively. These values were attributed to the addition of water from smectite dewatering during the smectite–illite (S–I) transformation, which produces water enriched in ^{18}O and depleted in D [25,26]. Because our porewater samples from KMV#10 show the same trends in $\delta^{18}O$ and δD values with respect to Cl⁻ concentrations, KMV#10 also was affected by water derived from clay mineral dehydration. Indeed, this process has previously been reported for other mud volcanoes in the Kumano basin (KMV#2–11) [13].

However, there are other possible source fluids beside those from the S–I transformation. Nishio et al. [16] inferred that Li isotope ratios in porewater of the drilled core from KMV#5 indicate temperatures as high as 310 °C, which is significantly higher than the S–I conversion temperature range of 60–150 °C. They suggested that a portion of fluid was derived from the periodic injection of deep-seated fluid accumulated in the corner of the serpentinized forearc mantle wedge, transported upward along a thrust fault [16]. Modeling of the water circulation in mud volcanoes of the Kumano basin has suggested that the fluids in the mud volcano sediment are derived by S–I transformation in the accretionary prism and decomposition of basaltic saponite in the subducting slab (Figure 8) [13]. In sum, the fluid in the mud volcanoes of the Kumano basin appears to originate in or beneath the accretionary prism underlying the Kumano forearc basin sediment.

The sediment samples from KMV#5 and KMV#10 were enriched in the clay size fraction compared to the reference sediment from the Kumano basin. The average composition of the clay-size minerals in the mud volcano sediments was 49% smectite, 25% illite, 15% quartz, and 11% chlorite, whereas in the reference sediment the clay-size minerals averaged 30% illite, 29% quartz, 23% smectite, and 18% chlorite. Interestingly, the sediment samples from KMV#5 and KMV#10 had very similar X-ray diffractograms, clay mineral compositions, expandability, and illite contents in the I/S mixed layer despite being about 30 km apart (Figure 1). This similarity indicates that these mud volcanoes are rooted in the same source sequence.

Sediments of the Kumano basin have also been sampled at Integrated Ocean Drilling Program (IODP) Site C0002, approximately 30 km south of KMV#5 (Figure 1) [18]. Because the clay-size mineral compositions at Site C0002 were estimated by the same methods as in this study [19,20], they can be compared directly with the results of this study. At Site C0002, the basin sediment shallower than 922 m below the seafloor (mbsf) contains Pleistocene nannofossils [27]. The sediment below 922 mbsf was interpreted as a boundary between accreted trench turbidites and muddy slope-apron deposits [27]. In sediments below 922 mbsf, this unit was assigned a late Miocene age on the basis of a nannofossil event [27]. In the basin sediment above 826 mbsf at Site C0002, illite is the dominant mineral in the clay-size fraction (~35–38%), as it is at the reference site of this study (30%). Between 834 and 922 mbsf, the clay-size fraction consists of smectite (36%), illite (35%), chlorite (16%), quartz (9%), and kaolinite (4%). Over the upper 922 m of the core, the expandability of the I/S mixed layer averages 60%. In the upper accretionary prism sediments below 922 mbsf at Site C0002, smectite is the dominant mineral in the clay-size fraction (41% average, 60% maximum), followed by illite (31%), chlorite (15%), quartz (6%), and kaolinite (5%). Smectite is likewise the dominant mineral (average 49%, maximum 59%) at KMV#5 and KMV#10, and the average expandability at KMV#5 and KMV#10 (67%) is close to that at Site C0002 below 922 m (69%).

These similarities suggest that the mud volcano sediment is derived from the upper accretionary prism rather than the Kumano basin. However, the mud volcano sediment and the accretionary prism sediment at Site C0002 appear to have conflicting ages. In the accretionary prism sediment of Site C0002, the maximum nannofossil age of 5.90 Ma corresponds to the late Miocene [27], whereas the nannofossils at KMV#5 are of late early to early middle Miocene age (13.6–18.2 Ma) [12]. The correspondence between this older age and the formation of abandoned forearc basins in the Shimanto accretionary belt on the Kii Peninsula led Morita et al. [12] to suggest that the mud volcano sediment was derived from the bottom of an old forearc basin. They reported that the deep structure of the Kumano Basin is divided into a northern zone consisting of three anticlines and a southern zone consisting of a large sedimentary basin that is bounded by a newly uplifted outer arc high. Site C0002 is in the southern zone, and the mud volcanoes of this study are in the northern zone (Figure 8). Thus, it is conceivable that the forearc basin sediment erupting in the mud volcanoes is older than the upper accretionary prism sediment at Site C0002. In sum, the evidence shows that the clay mineral composition of the mud volcano sediment differs from that of the Pleistocene basin sediments in the Kumano Basin and suggests that the mud volcano sediment originated in older sediments beneath the Pleistocene basin sediments.

Sharpness Ratios suggest that the mud volcano sediments have higher illite crystallinity, and hence higher maturity, than sediment at the reference site [24]. The results are consistent with the idea that the mud volcano sediments were derived from deeply buried strata, whereas the reference site represents surface sediment in the Kumano basin. Furthermore, the presence in the mud volcano sediments of the I/S mixed layer, an indicator of diagenetic S–I transformation [28,29], suggests that this material underwent the S–I transformation. This transformation is considered to occur at temperatures above ~60 °C and to be kinetically or thermodynamically controlled [28–33]. On that basis, the percentage of illite layers in the S/I mixed layer has been used as a geothermometer (e.g., [28,29]). The illite contents in the samples from KMV#5 and KMV#10 were 19–38% (average 32%).

We cannot confirm beyond doubt that the I/S mixed layer is of authigenic origin. However, at Ocean Drilling Program (ODP) Site 808, in the western part of the Nankai Trough (Figure 1), illite first appears at a depth of 555 mbsf, where the estimated temperature was ~65 °C, and increases monotonically with depth, reaching the illite contents of the I/S mixed layer in the mud volcano sediments (19–38%) at the depth range of 700–950 mbsf, where the estimated temperature range was 80–105 °C [34]. If the temperature dependence of S–I diagenesis is the same in the mud volcano sediments as it is at Site 808 and the I/S mixed layer is of authigenic origin, the mud volcano sediments at KMV#5 and KMV#10 experienced temperatures above 80 °C. Note that the sediment emitted by a mud volcano might involve the sediments surrounding the diapir conduit via hydraulic fracturing through mud diapir intrusion [35]. In that case, the I/S mixed layer in shallow strata, in which the illite content is low, would dilute the illite content in the I/S mixed layer of the diapiric mud volcano sediments, and thus the observed illite content of the I/S mixed layer, as well as the estimated temperature, may be minimum values.

At IODP Site C0009 in the Kumano Basin about 25 km south of KMV#5 (Figure 1), the temperature at the boundary between the basin sediments and the underlying accretionary prism (1288 mbsf) was estimated at ~40 °C [36]. To have reached temperatures above 80 °C, then, the mud volcano sediment must have come from beneath the basin sediment in the accretionary prism. However, the fossil evidence from KMV#5 points instead to an origin from the bottom of the basin sediment [12]. There are two possible ways to reconcile an origin in the basin with the XRD evidence suggesting that the mud volcano sediments experienced temperatures above 65 °C. One is that some factor other than temperature is different between the mud volcanoes and Site 808. Although temperature is the most important factor in the S–I transformation, the reaction is affected by many other internal and external variables [34]. The other possibility is that the source of the mud volcano sediment had a higher temperature in the past. Considering that the mud volcanoes lie along anticlines related to formerly

active megasplay faults [12,14], it may be that their source sediment was once more deeply buried and later raised by subduction-related uplift.

Another question concerns the degree to which the depletion of Cl⁻ in porewater at KMV#5 and KMV#10 occurred in situ from the S–I transformation in the mud volcano sediments. This can be addressed by the following rough mass balance calculation: The Cl⁻ concentration of the original porewater before the precipitation of methane hydrate is assumed to be ~150 mM (ca. 70% depletion) [15]. To produce the maximum depletion of porewater Cl⁻ of ca. 70% in sediment with a porosity of 53% (the minimum porosity measured in cores PC13 and PC14) requires the production of ca. 0.37 g of water per cubic centimeter of sediment. Smectite in marine sediment has been found to bind from 17.7 wt % to 27 wt % water [37,38], depending on environmental conditions. Assuming a value of 20% bound water on smectite, it would take 1.9 g smectite/cm^3 sediment to produce 0.37 g water/cm^3 sediment. Given the maximum bulk density (2.1 g/cm^3) and the minimum porosity (53%) of the sediments measured in cores PC13 and PC14, 1.9 g smectite/cm^3 sediment exceeds the dry bulk density (1.6 g/cm^3). Even if the original porosity of the source layer sediment was 30%, the dry bulk density is 1.8 g/cm^3, which is still lower than the required smectite volume. Consequently, the smectite contents in the mud volcano sediment are too small to produce the observed dilution of Cl⁻ in porewater by clay diagenesis in situ. This conclusion is consistent with the notion that the fluids in the mud volcano sediment are derived from the accretionary prism and subducting slab at depths below the source layer of the mud volcano sediment (Figure 8) [12].
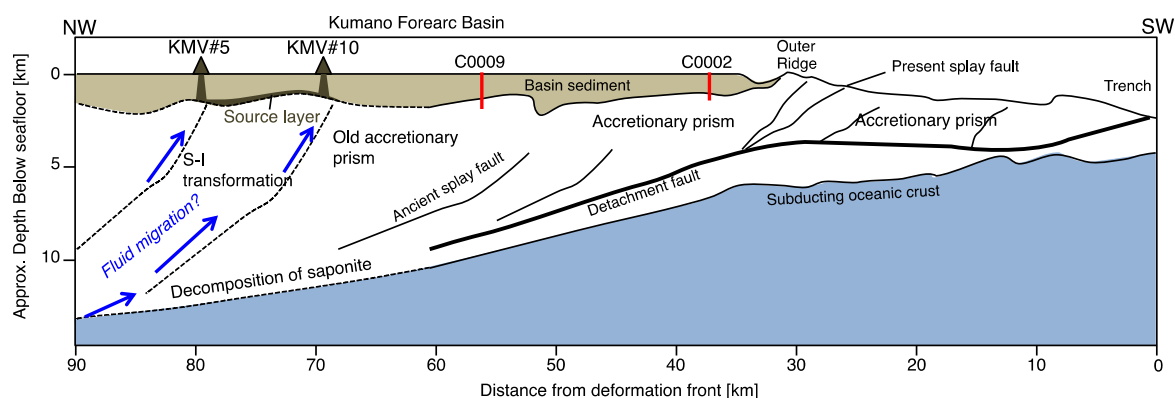

Figure 8. Sectional view of the Kumano forearc basin showing the origin of mud volcano sediments (source layer) and fluid migration from the old accretionary prism. Red bars indicate the locations of IODP Sites C0002 and C0009.

6. Conclusions

We determined the clay mineral compositions of sediment from submarine mud volcanoes, MV#5 and MV#10, in the Kumano forearc basin, Nankai Trough, by X-ray diffraction analysis. The sediment samples from KMV#5 and KMV#10 had very similar X-ray diffractograms, clay mineral compositions, expandability, and illite contents in the I/S mixed layer despite being about 30 km apart. The similar compositions in two mud volcanoes in the Kumano basin indicate that these mud volcanoes in the basin are rooted in the same source sequence.

These clay mineral compositions in the mud volcano sediment differed from those in Pleistocene basin sediment at Integrated Ocean Drilling Program Site C0002, in the southern part of the Kumano basin, suggesting that the mud volcano sediment originated beneath the Pleistocene sediment. Because the mud volcanoes are in the northern part of the Kumano basin where sediment deposits are older, it is conceivable that the source sequence of the mud volcano sediments is older than the Pleistocene basin sediments as well as the upper accretionary prism at IODP Site C0002 located in the southern part of the Kumano basin. The illite content in the illite–smectite mixed layer averaged 32% in the

mud volcano sediment, which implies that the sediment experienced temperatures above 60 °C that promoted the smectite-to-illite transformation. However, porewater extracted from the mud volcano sediment had Cl⁻ concentrations roughly half that of seawater and proportional enrichment in ^{18}O and depletion in D in porewater, indicating that dehydration reactions of clay minerals had previously occurred in a deeply buried sedimentary layer. The smectite and illite contents (<60%) of the clay-size fraction in the mud volcano sediment are too small to have produced the observed dilution of Cl⁻ in porewater by clay diagenesis in situ. Thus, fluids derived from clay dewatering must have originated from more in depth than the source of the mud volcano sediment.

Author Contributions: A.I. designed and performed the experiment and wrote the paper. K.I. technically supported the XRD analysis. U.T. conceived the chemical analysis of porewater and technically supported the isotopic analyses. J.A. was Chief Scientist of the research cruise and analyzed physical properties of the sediment samples. F.I. wrote the paper with A.I.

Conflicts of Interest: The authors declare no conflict of interest.

References

1. Dimitrov, L.I. Mud volcanoes—The most important pathway for degassing deeply buried sediments. *Earth-Sci. Rev.* **2002**, *59*, 49–76. [CrossRef]

2. Wallmann, K.; Drews, M.; Aloisi, G.; Bohrmann, G. Methane discharge into the Black Sea and the global ocean via fluid flow through submarine mud volcanoes. *Earth Planet. Sci. Lett.* **2006**, *248*, 544–559. [CrossRef]

3. Kaul, N.; Foucher, J.-P.; Heesemann, M. Estimating mud expulsion rates from temperature measurements on Håkon Mosby Mud Volcano, SW Barents Sea. *Mar. Geol.* **2006**, *229*, 1–14. [CrossRef]

4. Martin, J.B.; Kastner, M.; Henry, P.; LePichon, X.; Lallement, S. Chemical and isotopic evidence for sources of fluids in a mud volcano field seaward of the Barbados accretionary wedge. *J. Geophys. Res. Solid Earth* **1996**, *101*, 20325–20345. [CrossRef]

5. Dahlmann, A.; de Lange, G.J. Fluid-sediment interactions at Eastern Mediterranean mud volcanoes: A stable isotope study from ODP Leg 160. *Earth Planet. Sci. Lett.* **2003**, *212*, 377–391. [CrossRef]

6. Hensen, C.; Wallmann, K.; Schmidt, M.; Ranero, C.R.; Suess, E. Fluid expulsion related to mud extrusion off Costa Rica—A window to the subducting slab. *Geology* **2004**, *32*, 201–204. [CrossRef]

7. Hensen, C.; Nuzzo, M.; Hornibrook, E.; Pinheiro, L.M.; Bock, B.; Magalhaes, V.H.; Brückmann, W. Sources of mud volcano fluids in the Gulf of Cadiz—Indications for hydrothermal imprint. *Geochim. Cosmochim. Acta* **2007**, *71*, 1232–1248. [CrossRef]

8. Pape, T.; Geprägs, P.; Hammerschmidt, S.; Wintersteller, P.; Wei, J.; Fleischmann, T.; Bohrmann, G.; Kopf, A.J. Hydrocarbon seepage and its sources at mud volcanoes of the Kumano forearc basin, Nankai Trough subduction zone. *Geochem. Geophys. Geosyst.* **2014**, *15*, 2180–2194. [CrossRef]

9. Jurado-Rodriguez, M.J.; Martinez-Ruiz, F. Some clues about the Napoli and Milano mud volcanoes from an integrated log-core approach. In *Proceedings of the Ocean Drilling Program Scientific Results*; Robertson, A.H.F., Emeis, K.-C., Richter, C., Camerlenghi, A., Eds.; Drilling Program: College Station, TX, USA, 1998; Volume 160, pp. 607–624.

10. Schulz, H.-M.; Emeis, K.-C.; Volkmann, N. Organic carbon provenance and maturity in the mud breccia from the Napoli mud volcano: Indicators of origin and burial depth. *Earth Planet. Sci. Lett.* **1997**, *147*, 141–151. [CrossRef]

11. Alaoui Mhammedi, N.; El Moumni, B.; El Hmaidi, A.; Raissouni, A.; El Arrim, A. Mineralogical and geochemical study of mud volcanoes in north Moroccan Atlantic margin. *Afr. J. Environ. Sci. Technol.* **2008**, *2*, 387–396.

12. Morita, S.; Ashi, J.; Aoike, K.; Kuramoto, S. Evolution of Kumano Basin and Sources of Clastic Ejecta and Pore Fluid in Kumano Mud volcanoes, Eastern Nankai Trough. In Proceedings of the International Symposium on Methane Hydrates and Fluid Flow in Upper Accretionary Prisms (Prism Fluid 2004), Kyoto, Japan, 9 March 2004.

13. Menapace, W.; Völker, D.; Kaul, N.; Tryon, M.D.; Kopf, A.J. The role of mud volcanism and deep-seated dewatering processes in the Nankai Trough accretionary prism and Kumano Basin, Japan. *Geochem. Geophys. Geosyst.* **2017**, *18*, 2486–2509. [CrossRef]

14. Tsuji, T.; Ashi, J.; Strasser, M.; Kimura, G. Identification of the static backstop and its influence on the evolution of the accretionary prism in the Nankai Trough. *Earth Planet. Sci. Lett.* **2015**, *431*, 15–25. [CrossRef]

15. Ijiri, A.; Inagaki, F.; Kubo, Y.; Adhikari, R.R.; Hattori, S.; Hoshino, T.; Imachi, H.; Kawagucci, S.; Morono, Y.; Ohtomo, Y.; et al. Deep-biosphere methane production stimulated by geofluids in the Nankai accretionary complex. *Sci. Adv.* **2018**, *4*. [CrossRef]

16. Nishio, Y.; Ijiri, A.; Toki, T.; Morono, Y.; Tanimizu, M.; Nagaishi, K.; Inagaki, F. Origins of lithium in submarine mud volcano fluid in the Nankai accretionary wedge. *Earth Planet. Sci. Lett.* **2015**, *414*, 144–155. [CrossRef]

17. Manheim, F.T.; Sayles, F.L. Composition and origin of interstitial waters of marine sediments, based on deep sea drill cores. In *The Sea, Volume 5: Marine Chemistry*; Goldberg, E.D., Ed.; Wiley Interscience: New York, NY, USA, 1974; pp. 527–568.

18. Itai, T.; Kusakabe, M. Some practical aspects of an on-line chromium reduction method for D/H analysis of natural waters using a conventional IRMS. *Geochem. J.* **2004**, *38*, 435–440. [CrossRef]

19. Guo, J.; Underwood, M.B. Data report: Clay Mineral Assemblages from the Nankai Trough Accretionary Prism and the Kumano Basin, IODP Expeditions 315 and 316, NanTroSEIZE Stage 1. Available online: http://publications.iodp.org/proceedings/314_315_316/ERR/CHAPTERS/314315316_202.PDF (accessed on 15 June 2018).

20. Underwood, M.B.; Basu, N.; Steurer, J.; Udas, S. Data report: Normalization factors for semiquatitative X-ray diffraction analysis, with application to DSDP site 297, Shikoku Basin. In *Proceedings of the ODP, Science Results, 190/196*; Mikida, H., Moore, G.F., Taira, A., Becker, K., Moore, J.C., Klaus, A., Eds.; Ocean Drilling Program: College Station, TX, USA, 2003; pp. 1–28.

21. Biscaye, P.E. Mineralogy and sedimentation of recent deep-sea clay in the Atlantic Ocean and adjacent seas and oceans. *Geol. Soc. Am. Bull.* **1965**, *76*, 803–832. [CrossRef]

22. Moore, D.M.; Reynolds, R.C., Jr. *X-ray Diffraction and the Identification and Analysis of Clay Minerals*, 2nd ed.; Oxford University Press: New York, NY, USA, 1997; pp. 270–276.

23. Rettke, R.C. Probable burial diagenetic and provenance effects on Dakota Group clay mineralogy, Denver Basin. *J. Sediment. Petrol.* **1981**, *51*, 541–551. [CrossRef]

24. Weaver, C.E. Possible uses of clay minerals in search for oil. *AAPG Bull.* **1960**, *44*, 1505–1518.

25. Kastner, M.; Elderfield, H.; Martin, J.B. Fluids in convergent margins: What do we know about their composition, origin, role in diagenesis and important for oceanic chemical fluxes? *Philos. Trans. R. Soc. Lond.* **1991**, *A335*, 243–259. [CrossRef]

26. Yeh, H.W. D/H Ratios and Late-Stage Dehydration of Shales during Burial. *Geochim. Cosmochim. Acta* **1980**, *44*, 341–352. [CrossRef]

27. Kinoshita, M.; Tobin, H.; Ashi, J.; Kimura, G.; Lallemant, S.; Screaton, E.J.; Curewitz, D.; Masago, H.; Moe, K.T.; The Expedition 314/315/316 Scientists. *Proceedings of the Integrated Ocean Drilling Program, 314/315/316*; Ocean Drilling Program: College Station, TX, USA, 2009.

28. Hower, J.; Eslinger, E.; Hower, M.E.; Perry, E.A. Mechanism of burial metamorphism of argillaceous sediment: 1. Mineralogical and chemical evidence. *GSA Bull.* **1976**, *87*, 725–737. [CrossRef]

29. Pytte, A.M.; Reynolds, R.C. The thermal transformation of smectite to illite. In *Thermal History of Sedimentary Basins*; Naeser, N.D., McCulloh, T.H., Eds.; Springer: Berlin, Germany, 1989; pp. 133–140.

30. Perry, E.A.; Hower, J. Late-stage dehydration in deeply buried pelitic sediments. *AAPG Bull.* **1972**, *56*, 2013–2021.

31. Eberl, D.; Hower, J. Kinetics of illite formation. *Geol. Soc. Am. Bull.* **1976**, *87*, 1326–1330. [CrossRef]

32. Freed, R.L.; Peacor, D.R. Geopressured shale and sealing effect of the smectite to illite transition. *AAPG Bull.* **1989**, *73*, 1223–1232.

33. Huang, W.L.; Longo, J.M.; Pevear, D.V. An experimentally derived kinetic model for smectite-to-illite conversion and its use as a geothermometer. *Clays Clay Miner.* **1993**, *41*, 162–177. [CrossRef]

34. Underwood, M.B.; Pickering, K.; Gieskes, J.M.; Kastner, M.; Orr, R. Sediment geochemistry, clay mineralogy, and diagenesis: A synthesis of data from Leg 131, Nankai Trough. In *Proceedings ODP Science Results, 131*; Hill, I.A., Taira, A., Firth, J.V., Berner, U., Bruückmann, W., Byrne, T., Chabernaud, T., Fisher, A., Foucher, J.-P., Gamo, T., et al., Eds.; Ocean Drilling Program: College Station, TX, USA, 1993; pp. 343–363.

35. Ujiié, Y. Mud diapirs observed in two piston cores from the landward slope of the northern Ryukyu Trench, northwestern Pacific Ocean. *Mar. Geol.* **2000**, *163*, 149–167. [CrossRef]

36. Saffer, D.; McNeill., L.; Byrne, T.; Araki, E.; Toczko, S.; Eguchi, N.; Takahashi, K.; The Expedition 319 Scientists. *Proceedings of the Integrated Ocean Drilling Program 319*; Ocean Drilling Program: College Station, TX, USA, 2010.

37. Saffer, D.M.; Tobin, H.J. Hydrogeology and mechanics of subduction zone forearcs: Fluid flow and pore pressure. *Annu. Rev. Earth Planet. Sci.* **2011**, *39*, 157–186. [CrossRef]

38. Hüpers, A.; Kopf, A.J. Effect of smectite dehydration on pore water geochemistry in the shallow subduction zone: An experimental approach. *Geochem. Geophys. Geosyst.* **2012**, *13*. [CrossRef]